My results

Time Crystals Induced by Cavity (not published yet)

Subharmonic response in a driven all-to-all Ising model. Top: ⟨Z⟩(t), photon number, and 2T-stroboscopic FFT display a pronounced ω/2 peak (period-doubling) for the Hamiltonian in Eq. (1). Bottom: heatmap of the ω/2 FFT amplitude from ⟨Z⟩ versus h/h_0 and J/J_0, delineating a broad lobe of robust time-crystal behavior.

With Prof. Michael Kolodrubetz, I investigated how cavity-mediated long-range interactions can generate persistent, period-doubled correlations without external driving. By mapping between Majorana formulations and an Ising-spin description, we identified observables---stable long-time oscillations and correlations---that survive photon loss and are accessible in realistic measurements. The resulting time-independent Hamiltonian realizes the phenomenology of discrete time crystals via self-organized feedback, connecting Floquet physics to cavity QED and highlighting collective interactions as a resource for nonequilibrium order.

- 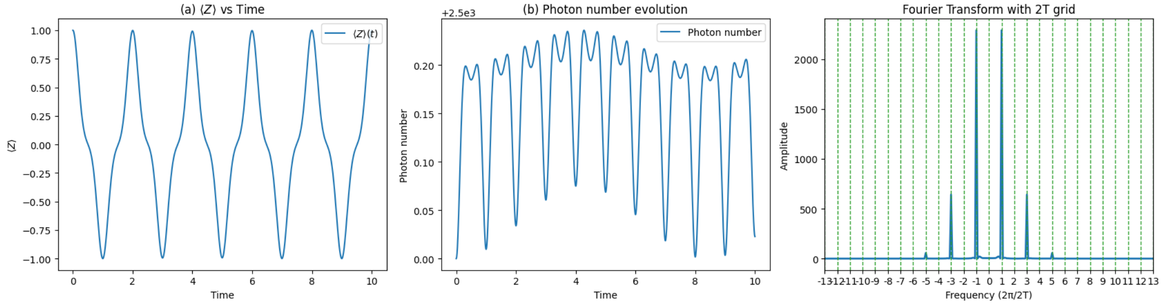

- 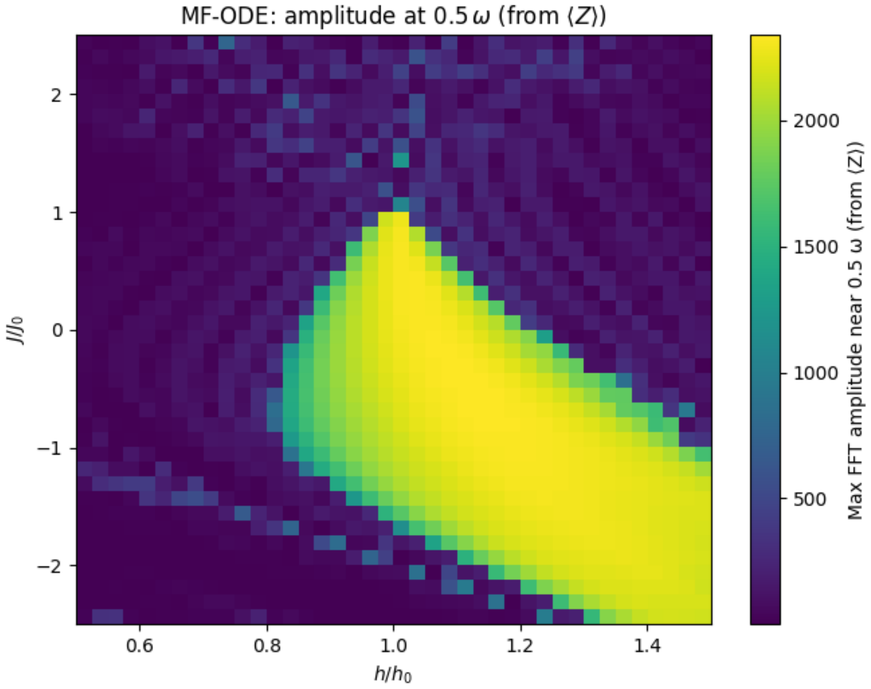

(Effect of Trap in) Quantum Kicked Rotor with Interaction

Working with Prof. Chuanwei Zhang and Prof. Subhadeep Gupta’s group (UW), I studied ultracold atomic gases under quasi-periodic kicks as a controlled setting for Anderson metal--insulator physics. Using a Bose--Einstein condensate in an optical lattice, we quantified how repulsive interactions and realistic trapping potentials reshape transport. Mean-field simulations matched experiment and revealed a distinct subdiffusive regime that departs from single-particle predictions. From data--theory comparisons I extracted critical exponents indicative of an interaction-driven transition. This clarifies how many-body effects govern dynamical phases in driven disordered systems and provides a blueprint for using kicks as tunable probes of transport universality.

- 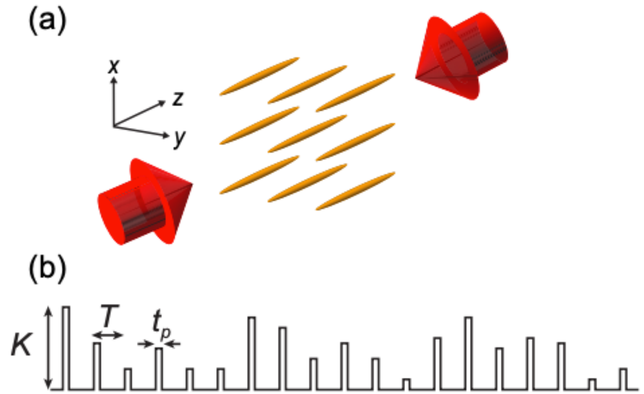

- Experimental realization of the quantum kicked rotor. (a) Ultracold atoms interact with a pulsed, far-detuned standing wave formed by two counter-propagating laser beams (axes x–y–z). The optical lattice imparts the “kicks.” (b) Pulse train with period (T), duration (t_p), and kick strength (K) setting the effective stochasticity.
-

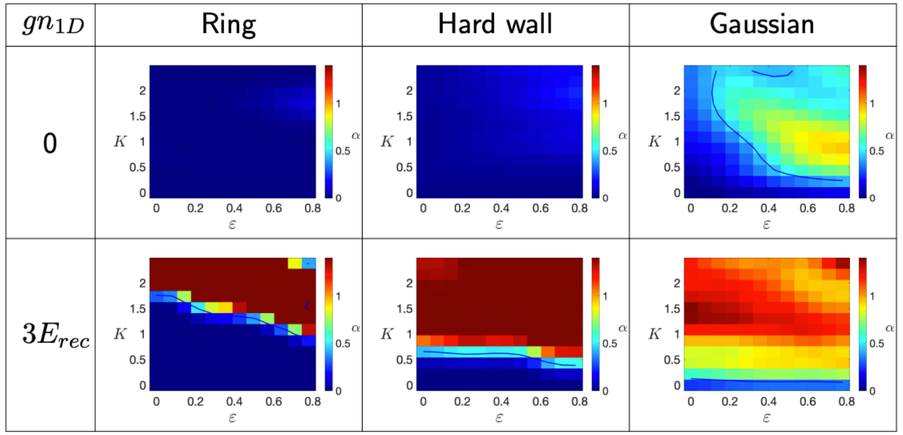

- Comparison across setups. This shows heatmaps of diffusion exponent (α) versus kick strength (K) and detuning (\ ε) for three geometries (Ring, Hard wall, Gaussian) and two interaction cases (($gn_{1\mathrm{D}}=0$) and ($3E_{\mathrm{rec}}$)).
-

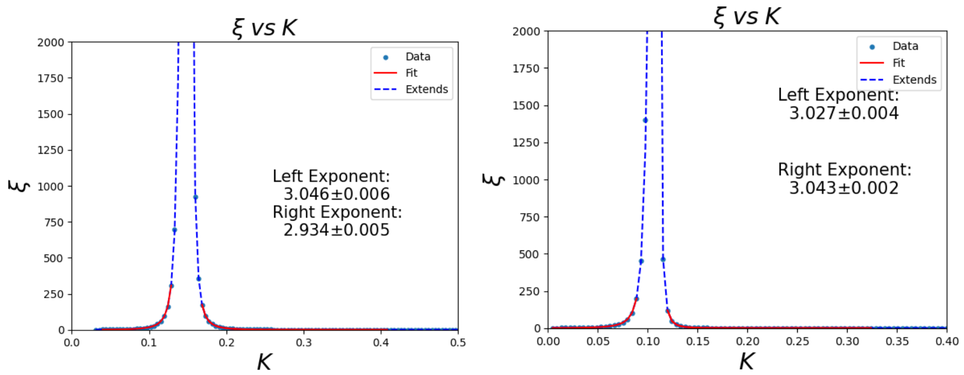

Localization length ($\xi(K)$) for **Ring and Hard-wall** cases; fits near the delocalization point yield critical exponents ($\nu!\approx3$) on each side, indicating robust, setup-insensitive behavior.

Finding Quantum Error Correction code

```
In collaboration with Prof.\ Bei Zeng,
Prof.\ Yiu-Tung Poon, and Dr.\ Chao
Zhang, I developed a framework that
analyzes quantum codes through the off-
diagonal Knill--Laflamme conditions. We
introduced a \emph{signature vector}
with locally unitary--invariant norm $
\lambda^{*}$, which diagnoses error-
correcting capability and guides code
discovery. Using this tool, we
uncovered new non-additive code
families, including $((6,2,3))$ and $
((7,2,3))$, and charted their
relationships on a Stiefel-manifold
picture of code spaces. The method
supplies analytic traction in high-
dimensional landscapes and suggests
routes to robust, low-overhead
protocols.
```

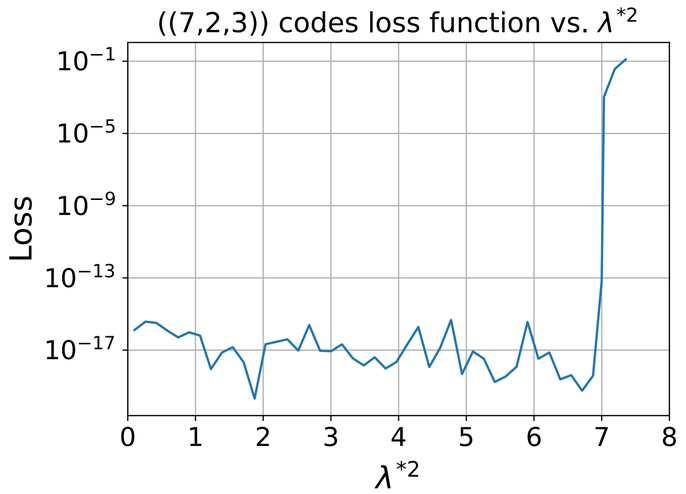

$$
\begin{aligned}
c_0 &= \frac{\sqrt{\sqrt{7}\lambda^* + 8}}{8}, \\
c_1 &= -\frac{\sqrt{\sqrt{7}\lambda^*}}{8}, \\
c_4 &= -\sqrt{3}c_1, \\
c_3 &= \frac{2}{5}\left(\sqrt{7}c_0 \pm \sqrt{7c_0^2 - \frac{15\sqrt{7}\lambda^*}{64}}\right), \\
c_2 &= -2c_3 + \sqrt{7}c_0
\end{aligned}
$$

Loss landscape for (((7,2,3))) nonadditive codes versus signature-vector magnitude (λ^{*2}) (log scale). The KL-violation loss remains at machine precision across most (λ^{*2}), then rises sharply near ($ \lambda^{2}!=7$), *marking the boundary where no code simultaneously satisfies the constraints for this target (λ^*).*